Spatial-temporal variations of ecological vulnerability in the Tarim River Basin, Northwest China

BAI Jie[1,2,3], LI Junli[1,2,3*], BAO Anmin[1,2,3], CHANG Cun[1,2,3]

[1] State Key Laboratory of Desert and Oasis Ecology, Xinjiang Institute of Ecology and Geography, Chinese Academy of Sciences, Urumqi 830011, China;
[2] Key Laboratory of GIS & RS Application Xinjiang Uygur Autonomous Region, Urumqi 830011, China;
[3] University of Chinese Academy of Sciences, Beijing 100049, China

Abstract: As the largest inland river basin of China, the Tarim River Basin (TRB), known for its various natural resources and fragile environment, has an increased risk of ecological crisis due to the intensive exploitation and utilization of water and land resources. Since the Ecological Water Diversion Project (EWDP), which was implemented in 2001 to save endangered desert vegetation, there has been growing evidence of ecological improvement in local regions, but few studies have performed a comprehensive ecological vulnerability assessment of the whole TRB. This study established an evaluation framework integrating the analytic hierarchy process (AHP) and entropy method to estimate the ecological vulnerability of the TRB covering climatic, ecological, and socioeconomic indicators during 2000–2017. Based on the geographical detector model, the importance of ten driving factors on the spatial-temporal variations of ecological vulnerability was explored. The results showed that the ecosystem of the TRB was fragile, with more than half of the area (57.27%) dominated by very heavy and heavy grades of ecological vulnerability, and 28.40% of the area had potential and light grades of ecological vulnerability. The light grade of ecological vulnerability was distributed in the northern regions (Aksu River and Weigan River catchments) and western regions (Kashgar River and Yarkant River catchments), while the heavy grade was located in the southern regions (Kunlun Mountains and Qarqan River catchments) and the Mainstream catchment. The ecosystems in the western and northern regions were less vulnerable than those in the southern and eastern regions. From 2000 to 2017, the overall improvement in ecological vulnerability in the whole TRB showed that the areas with great ecological improvement increased by 46.11%, while the areas with ecological degradation decreased by 9.64%. The vegetation cover and potential evapotranspiration (PET) were the obvious driving factors, explaining 57.56% and 21.55% of the changes in ecological vulnerability across the TRB, respectively. In terms of ecological vulnerability grade changes, obvious spatial differences were observed in the upper, middle, and lower reaches of the TRB due to the different vegetation and hydrothermal conditions. The alpine source region of the TRB showed obvious ecological improvement due to increased precipitation and temperature, but the alpine meadow of the Kaidu River catchment in the Middle Tianshan Mountains experienced degradation associated with overgrazing and local drought. The improved agricultural management technologies had positive effects on farmland ecological improvement, while the desert vegetation in oasis-desert ecotones showed a decreasing trend as a result of cropland reclamation and intensive drought. The desert riparian vegetation in the lower reaches of the Tarim River was greatly improved due to the implementation of the EWDP, which has been active for tens of years. These results provide comprehensive knowledge about

Corresponding author: LI Junli (lijl@ms.xjb.ac.cn)
Received 2021-01-26; revised 2021-07-23; accepted 2021-07-29

ecological processes and mechanisms in the whole TRB and help to develop environmental restoration measures based on different ecological vulnerability grades in each sub-catchment.

Keywords: ecological vulnerability; ecological improvement; ecological degradation; AHP-entropy method; climate change; human activities; Tarim River Basin

1 Introduction

In the context of climate change and human activities, a comprehensive quantification of the degrees to which natural and human systems experience hazards, disturbances, and pressures has been widely considered (Beroya-Eitner, 2016). In arid and semi-arid areas where the desert ecosystem is fragile to climate change and the water condition is a dominating factor for ecosystems (Huang et al., 2016), intensive human activities aggravate water resource crises (Groisman et al., 2018) and the deterioration of the ecological environment (Bestelmeyer et al., 2015). Therefore, it is essential to evaluate ecosystem vulnerability to achieve sustainable economic development and environmental protection in arid and semi-arid regions.

The concept of 'vulnerability' was previously used for social science and recently used in ecological fields (e.g., ecological vulnerability, environmental vulnerability, and ecosystem vulnerability) (Beroya-Eitner, 2016). It has various similar expressions (e.g., risk, sensitivity, and fragility) and inverse ideas (e.g., resilience, adaptability, adaptive capacity, and stability) (Hinkel, 2011). In the context of ecology, 'vulnerability' refers to the possibilities of an ecosystem suffering from hazards, disturbances, or pressures over time and space (Williams and Kaputska, 2000) or the risks of severe destruction to the ecosystem (Nguyen et al., 2016). However, how to establish an evaluation criteria system and develop an evaluation model is a key to ecosystem vulnerability assessment. The key indicators of ecosystem assessment vary in the context of space, time, and conditions, so these indicators include not only the current status of socioeconomic indicators or ecological indicators but also indicators with spatial-temporal information that can describe the dynamic variations in an ecosystem at different spatial scales or time scales. With the development of remote sensing (RS) and geographic information system (GIS), land surface parameters such as land use/land cover (LULC), land surface temperature, normalized difference vegetation index (NDVI), vegetation coverage, and topography condition have been widely used as the key indicators that describe the changes in ecosystem status and processes (Nandy et al., 2015; Zou and Yoshino, 2017; Zhao et al., 2018; Yu et al., 2020). Additionally, many models and methods have been developed for the quantitative assessment of ecological vulnerability, such as the analytic hierarchy process (AHP) (Nguyen et al., 2016), principal component analysis (PCA) (Nandy et al., 2015; Zou and Yoshino, 2017), entropy method (Ludovisi, 2014; Zhao et al., 2018), fuzzy assessment model (Enea and Salemi, 2001), grey model (Silva et al., 2016), and artificial neural network model (Dzeroski, 2001). However, most of these models determined the weights of the selected indices based on prior knowledge or empirical methods. If some of these weight coefficients are set improperly, the model will overestimate or underestimate the ecological effects during the assessment processes. The entropy method, with a strong theoretical basis of mathematics, determines the weight of the ecological indicators according to the degree of variation of each index (Ludovisi, 2014). Compared with various subjective weighting models, the greatest advantage of the entropy method is that it removes the effect of human interference on the weight of indicators (Zhu et al., 2020); however, it ignores the knowledge and experience of experts as well as the intentions and preferences of decision-makers from reality. The AHP method is a mathematical technique used to develop a set of weights by making pairwise comparisons among the criteria into a hierarchical structure (Saaty, 2001). It can comprehensively consider experts' opinions and judgements, and it is commonly integrated into objective weight methods to add the knowledge and experience of the experts in decision-making (Du and Gao,

2020; Nyimbili and Erden, 2020). Therefore, it is necessary to combine the AHP and entropy methods to derive the advantages of both subjective and objective methods, and this approach could reasonably recognize the effects of each indicator on environmental vulnerability.

The Tarim River Basin (TRB) is a typical inland river basin in Northwest China that is known for its arid and semi-arid climate and fragile ecosystems. The ecological environment of the TRB has continued to deteriorate since 1960 due to climate change and intensive human activities (Xu et al., 2010). The expansion of agricultural oases represents the aggravation of deforestation and the increase in irrigation, while excessive development and inefficient utilization of water resources have led to a water crisis and ecological degradation in this region, affecting the sustainable development of social, economic, and natural ecosystems. To restore the desert ecosystem and improve the ecological quality in the riparian zones, the local government had launched the ecological water diversion project (EWDP) to transport water to the middle and lower reaches of the Tarim River and its tributary system since 2001 (Bao et al., 2017). Many studies have evaluated the ecological effects of the EWDP using field investigations, site observations (Chen et al., 2010; Hao and Li, 2014), and remote sensing monitoring (Bao et al., 2017; Guo et al., 2017), but the results showed very different extents and ranges of influences on the environmental quality of the Tarim River after the implementation of ecological restoration (Chen et al., 2010; Hao and Li, 2014; Ling et al., 2019). Xue et al. (2018) found that the environmental quality of the TRB was not improved, and several regions of the TRB severely deteriorated due to excessive agricultural water consumption and extensive economic development, without regard to the indicators of the ecological environment. In previous studies, more attention was given to the middle and lower reaches of the Tarim River, while the upstream regions as well as the fragility and sensitivity of the mountain ecosystem were not considered in the ecological vulnerability assessment. The main ecological problem in the TRB is the uncertainty of ecological vulnerability when it is involved in the interactions among the inland water cycle, eco-environment, and socioeconomic factors. Therefore, it is essential to establish a comprehensive indicator system including meteorological, hydrological, ecological, and economic parameters and to evaluate the ecological vulnerability at the basin scale for the TRB.

In this paper, an assessment index system using RS and GIS technology was established, and the parameters included ten indicators related to climate change, ecological environments, and socioeconomic conditions. Then, an evaluation framework based on the AHP-entropy method was used to estimate the ecological vulnerability of the TRB at the basin scale, and the spatial-temporal changes in the vulnerability grades and their driving factors were analyzed at the catchment scale during 2000–2017.

2 Materials and methods

2.1 Study area

The Tarim River, located in Xinjiang Uygur Autonomous Region of China, is the longest inland river (with a total length of 1321 km) in China (Deng et al., 2016). The TRB is surrounded by mountains on three sides, with the Tianshan Mountains to the north, the Karakoram Mountains to the west, and the Kunlun Mountains to the south. The Taklimakan Desert, the largest desert in China, covers the vast central region of the TRB (Fig. 1). The TRB has an extremely dry climate with a mean annual precipitation of 15–65 mm, an above-freezing temperature (AFT) of 10°C–12°C, and a potential evapotranspiration (PET) of 2000–3000 mm. The vegetation in the study area is densely distributed in alpine and oasis areas but sparsely distributed in the narrow riparian zone across the main and branch channels. The main land use types derived from the LULC map in 2017 included grassland, forestland, cropland, water body, build-up land, and other land use types (including Gobi, desert, bare land, bare rocks, gravels, and glaciers), whose areas accounted for 24.69%, 8.03%, 4.69%, 1.27%, 0.48% and 60.85% of the total area, respectively. Rainfall, seasonal snowfall, and glacier meltwater in mountainous areas are the major water sources in this inland water cycle. There are nine headstreams that flow into the main branch of

the Tarim River, splitting the whole TRB into nine sub-catchments and one Mainstream catchment (Fig. 1). Currently, only three headstreams (Hotan River, Yarkant River, and Aksu River) have hydraulic connections with the main branch of the Tarim River.

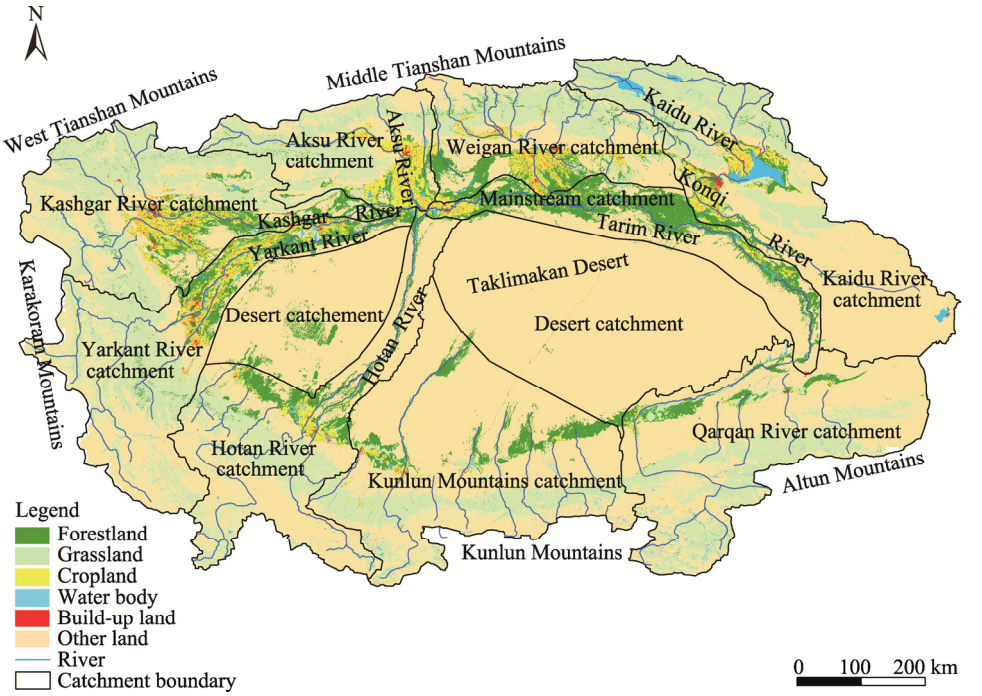

Fig. 1 Overview of the Tarim River Basin (TRB) as well as the area percentage of land use/land cover (LULC)

2.2 Derivation of ecological vulnerability indicators

In this study, ten indicators, including three climate indicators (precipitation, AFT, and PET), four ecological indicators (vegetation cover, soil erosion, landscape diversity, and water density), and three socioeconomic indicators (population density, food production, and livestock density), were selected. The computing formulas of these indicators are shown in Table S1. The variance inflation factors of these indicators were all lower than 10 (Table 1), which indicated that the collinearity of the indicators is in a reliable range (Zhao et al., 2018). The indicator 'landscape diversity' was generated by Fragstats software (version 4.2), and the other nine indicators were processed by ArcGIS and R software (version 3.5.2). Apart from the desert catchments, the nine catchments were used for ecological vulnerability assessment.

Table 1 Variance inflation factors for the selected ecological vulnerability indicators

Year	PRE	AFT	PET	LD	VC	WD	SE	FOOD	POP	LS
2000	1.3997	1.3097	1.2423	1.1830	1.2224	1.4130	1.3325	1.3839	1.2572	1.3570
2010	1.3523	1.3021	1.2488	1.1596	1.1811	1.3475	1.3520	1.3606	1.3301	1.4077
2017	1.3396	1.3137	1.2310	1.1637	1.1791	1.3282	1.3601	1.3517	1.5602	1.6395

Note: PRE, precipitation; AFT, above-freezing temperature; PET, potential evapotranspiration; LD, landscape diversity; VC, vegetation cover; WD, water density; SE, soil erosion; FOOD, food production; POP, population density; LS, livestock density.

2.2.1 Climate indicators

Daily meteorological data (including air temperature, sunshine hours, wind speed, and relative humidity) of stations in Xinjiang during 2000–2017 were acquired from China Meteorological Data Service Centre (http://data.cma.cn). These data were interpolated to a spatial scale of 10-km grids using the Meteorological Distribution System for High-Resolution Terrestrial Modeling (MicroMet) (Liston and Elder, 2006). The daily gridded PET dataset was calculated using the Penman-Monteith equation (Table S1) and the interpolated meteorological data. The daily maximum temperature

above 0°C was accumulated annually and called the AFT. The annual cumulative precipitation and PET were obtained from the daily gridded dataset. All the indicators were resampled to a resolution of 500 m using the bilinear method (Yu et al., 2020).

2.2.2 Ecological indicators

The monthly MOD13A1 enhanced vegetation index (EVI) product (Collection 6; 500 m×500 m) during 2000–2017 was acquired from the NASA Land Processes Distributed Active Archive Centre (https://lpdaac.usgs.gov). The annual EVI was calculated using the maximum value composite method, and the annual vegetation cover indicator was calculated by pixel dichotomy methods (Table S1).

The soil texture (sand, silt, and clay) data were came from the soil particle-size distribution dataset at the 1:100,000 scale (Wei et al., 2012), and the soil organic carbon data were downloaded from the World Soil Database (Version 1.2; resolution of 1 km×1 km) (Nachtergaele et al., 2009). The slope and aspect parameters were calculated from the Shuttle Radar Topography Mission (SRTM) Digital Elevation Model (DEM) product (http://srtm.csi.cgiar.org). The soil erosion indicator was estimated by the Revised Universal Soil Loss Equation (Table S1), which is an effective and widely used empirical model for estimating the soil erosion risk (Renard et al., 1991).

The LULC maps in 2000, 2010, and 2017, which were generated by the Chinese Academy of Sciences, were came from the China National Land Cover Database (ChinaCover) at a 30-m resolution (Wu et al., 2017). The ChinaCover based on Landsat TM/ETM and HJ satellite imagery employs an object-based approach with a large number of field data, and the overall accuracy is greater than 86% (Zhang et al., 2014). The six types of LULC shown in Figure 1 were extracted from the Level I of ChinaCover, which were consistent with the classes set by the United Nations Intergovernmental Panel on Climate Change (IPCC) (Zhang et al., 2014). In this study, forestland included shrubland, and wetland was reclassified into water body. The vector maps of LULC were first transformed to raster images with a pixel size of 500 m using the bilinear method, and then Shannon's diversity index was applied to estimate landscape diversity (Table S1).

The water availability of five administrative prefectures (Bayingol Mongolian Autonomous Prefecture, Aksu Prefecture, Kashgar Prefecture, Hotan Prefecture, and Kizilsu Kirgiz Autonomous Prefecture) in the TRB for 2000, 2010, and 2017 was obtained from the Xinjiang Water Resources Bulletin (http://slt.xinjiang.gov.cn/) issued by the Department of Water Resources of Xinjiang Uygur Autonomous Region (2000, 2010, 2017). The administrative boundary at a catchment scale was rasterized to a 500-m pixel size, and the density of water availability was partitioned into each pixel of different catchments. The proportion of river length and the water body area in each pixel were extracted from the LULC map. The weight of water availability in each pixel was calculated by the distance from the river, LULC, and slope (Lei et al., 2007).

2.2.3 Socioeconomic indicators

The population density, livestock density, and food production data in 46 counties or cities of the TRB were collected from the Xinjiang Statistical Yearbooks of 2000–2017 (Xinjiang Uygur Autonomous Region Bureau of Statistics, 2000–2017). The food production in this study included gain crops (wheat, maize, rice, and bean), oil crops, vegetation, potato, and melons. The food production (unit: t) was counted by food calories (unit: kcal) to unify the evaluation criteria of various crops (Table S1). We also unified the number of different livestock species (cattle, horse, sheep, donkey, and pig) into the standard number of sheep (Table S1). The ratios of the population density, livestock density, and food production data to the county (or city) area were calculated following the equations in Table S1, and then they were associated with attribution fields of county name in the vector data of the county (city)-level administrative boundary. The vector datasets of population density, livestock density, and food production were rasterized to raster datasets with a resolution of 500 m using the bilinear method.

2.3 Ecological vulnerability assessment

2.3.1 Standardization of indicators

To evaluate different indicators in dimensionless form, indicators that had positive and negative effects on the result were standardized as Equations 1 and 2 (Shi et al., 2018), respectively. The

calculations were as follows:

$$y_{ij} = \frac{x_{ij} - \min(x_j)}{\max(x_j) - \min(x_j)}, \quad (1)$$

$$y_{ij} = \frac{\max(x_j) - x_{ij}}{\max(x_j) - \min(x_j)}, \quad (2)$$

where y_{ij} is the standardized result of the i^{th} evaluating pixel on the j^{th} indicator; x_{ij} is the original value of the pixel; and $\min(x_j)$ and $\max(x_j)$ are the minimum and maximum of x_j, respectively. In this study, the indicators with positive effects were AFT, PET, soil erosion, population density, and livestock density, while the indicators with negative effects were precipitation, vegetation cover, landscape diversity, water density, and food production.

2.3.2 Calculating the weight of indicators

In this study, the AHP method was first adopted to allocate weights subjectively by allowing experts to evaluate the relative importance of indicators in pairs. Then, we applied the entropy method to obtain objective weights according to the degree of variation of each indicator. Finally, the integrated AHP-entropy method was used to get the final weight. The steps of the associated calculation were as follows:

Step 1: Calculating the subjective weights of the indicators with the AHP method.

The judgement matrix of pairwise comparisons was established according to the composite opinions of three experts from ecological, agricultural, and water resource management departments, and this approach adequately represents the local field experience (Xue et al., 2018). The consistency ratio (CR) was 0.067 in this study, which is less than 0.100, indicating that the matrix had a reasonable consistency (Saaty, 2001).

Step 2: Calculating the objective weights of the indicators with the entropy method.

We estimated the ten indicators according to the entropy method following the formulas below (Amiri et al., 2014; Pan et al., 2015). First, we defined the proportion of the standardization indicator according to Equation 3. Second, we calculated the entropy H_j and weight W_j^e of each indicator using Equations 4 and 5. The calculations were as follows:

$$p_{ij} = (1 + y_{ij}) / \sum_{i=1}^{m} (1 + y_{ij}), \quad (3)$$

$$H_j = -\left(\sum_{i=1}^{m} p_{ij} \ln p_{ij} \right) / \ln m, \quad (4)$$

$$W_j^e = \left(1 - H_j\right) / \left(n - \sum_{j=1}^{n} H_j \right), \quad (5)$$

where p_{ij} represents the proportion of the i^{th} pixel of the j^{th} indicator; H_j is the entropy of the j^{th} indicator; W_j^e is the weight of the j^{th} indicator; m is the total number of estimating pixels; and n is the number of evaluation indicators.

Step 3: Integrating AHP-entropy method of the indicators.

We calculated the overall combined weight value based on the AHP and entropy method as shown in Equation 6:

$$w_j = \frac{\sqrt{(w_j^a w_j^e)^2}}{\sum_{j=1}^{n} \sqrt{(w_j^a w_j^e)^2}}, \quad (6)$$

where w_j represents the combined weight; W_j^a is the subjective weight calculated from the AHP method; and w_j^e is the objective weight derived from the entropy method. Clearly, we designed $\sum_j w_j = 1$ and $w_j \geq 0$ for $j = 1, 2, \ldots, n$. The weights of the indicators are shown in Table 2.

Table 2 Weights of the selected ecological vulnerability indicators

Year	PRE	AFT	PET	LD	VC	WD	SE	FOOD	POP	LS
2000	0.1481	0.0888	0.0308	0.1509	0.2098	0.2524	0.0192	0.0964	0.0026	0.0009
2010	0.1456	0.0892	0.0322	0.1522	0.2041	0.2522	0.0241	0.0973	0.0022	0.0009
2017	0.1464	0.0886	0.0343	0.1536	0.1992	0.2537	0.0242	0.0974	0.0017	0.0009

2.3.3 Determining evaluation grades

We used the natural break points (Jenks) method (Zhao et al., 2018) to obtain the ecological vulnerability grade, which was implemented automatically by ArcGIS software. This method minimized intragroup variation and maximized intergroup variation. The grade of ecological vulnerability was reclassified into five degrees: potential (0.26–0.54), light (0.54–0.64), medium (0.64–0.69), heavy (0.69–0.75), and very heavy (0.75–0.85).

We classified "Up 1 grade" as when the ecological vulnerability grade transformed from one low level to one high level and "Up 2 grade" as when the ecological vulnerability grade transformed from one low level to two high levels. In contrast, we classified "Down 1 grade" as when the ecological vulnerability grade transformed from one high level to one low level and "Down 2 grade" as when the ecological vulnerability grade transformed from one high level to two low levels.

2.3.4 Geographical detection method (GDM)

The geographical detection method is a type of variance analysis that can detect spatial differentiation and reveal its driving factors (Wang et al., 2016); it has been successfully used to quantitatively analyze the driving factors of ecological vulnerability (Guo et al., 2020). In this study, we used the factor detector module to quantify the contribution of driving factor x explaining the spatial-temporal differentiation of ecological vulnerability by the q-value, which was calculated as follows:

$$q_x = 1 - \frac{SSW}{SST} = 1 - \frac{\sum_{h=1}^{L} N_h \sigma_h^2}{N\sigma^2}, \tag{7}$$

where q_x is the explanatory power of driving factor x for ecological vulnerability; SSW and SST are the within sum of squares in layer h and the total sum of squares, respectively; h (h=1, 2, …, L) is the category number of driving factor x; L is the number of categories; N_h and N are the numbers of units for layer h and the whole region, respectively; and σ_h^2 and σ^2 are the variances of ecological vulnerability in layer h and the whole region, respectively. The larger the q-value, the greater the explanatory power of driver x to ecological vulnerability.

To obtain continuous independent variables in the GDM, we converted the driving factors into discrete intervals using the natural break points (Jenks) method (Zhao et al., 2018) in ArcGIS software. The calculation of the GDM was performed in R software (version 3.5.2) using the 'geodetector' package.

3 Results

3.1 Spatial distribution of ecological vulnerability

The overall values of ecological vulnerability in the whole TRB slightly decreased from 0.686 (±0.090) to 0.666 (±0.096) during 2000–2017 (Fig. 2). This result indicated that the ecological environment in the whole TRB slightly improved in the past 18 a. As more than half of the study area is dominated by the desert and desertification regions, the overall grade of ecological vulnerability in the TRB remained at a relatively high level, and the averaged area with ecological vulnerability above the heavy grade level accounted for approximately 57.27% of the total area (Fig. 2d). The averaged area of the potential grade was the smallest, accounting for only 6.87% (Fig. 2d), and these regions were mainly distributed in mountainous grasslands or croplands along the riparian zone (Fig. 2a–c). From 2000 to 2017, the area proportion at the potential and light grades increased by 57.86% and 39.60%, respectively, while that at the heavy grade decreased by

25.83% (Fig. 2d). The area proportion at the medium and very heavy grade levels remained relatively stable with change rates of –5.61% and –5.97%, respectively, during the study period. Therefore, the ecological environment of the TRB was slightly improved, with continually increasing area at the potential and light grades, and decreasing area at the heavy grade.

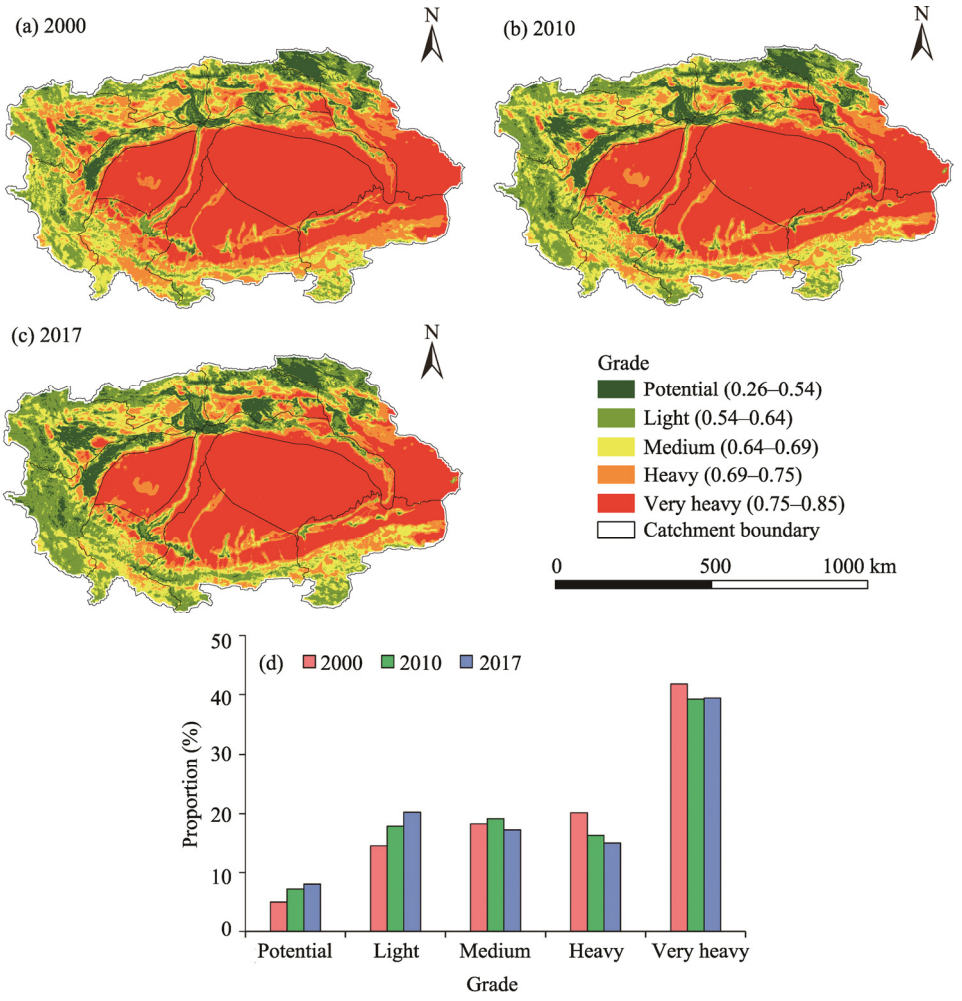

Fig. 2 Spatial distribution of ecological vulnerability grades in 2000 (a), 2010 (b), and 2017 (c), and the area proportion of ecological vulnerability grades distributed in 2000, 2010, and 2017 (d)

Comparing the spatial patterns of the ecological vulnerability grades in different catchments, the results showed overall downward trends from the upstream to the downstream of the catchments, from the mountainous areas to the alluvial plain areas, and from the west to the east of the TRB. The Yarkant River and Aksu River catchments in the upstream with abundant precipitation and glacier meltwater had better ecological environments with higher vegetation cover (Fig. 3). Especially in the Yarkant River catchment, approximately 52.84% of the catchment area was classified as being in the light grade in 2017 (Fig. 3b). However, the Kunlun Mountains catchment, with fragile regions of very heavy grade accounting for more than 50.00% of the total catchment area, had the worst ecological environment due to sparse vegetation and less river flow. The areas of potential and light grades obviously increased in the Yarkant River, Kashgar River, Hotan River, and Aksu River catchments, while those of the heavy grade significantly decreased in the Kashgar River and Yarkant River catchments from 2000 to 2017 (Fig. 3). The ecological vulnerability grade upgraded from medium to light in the Kashgar River and Weigan River catchments, while upgraded from heavy to medium in the Hotan River and Kaidu River catchments.

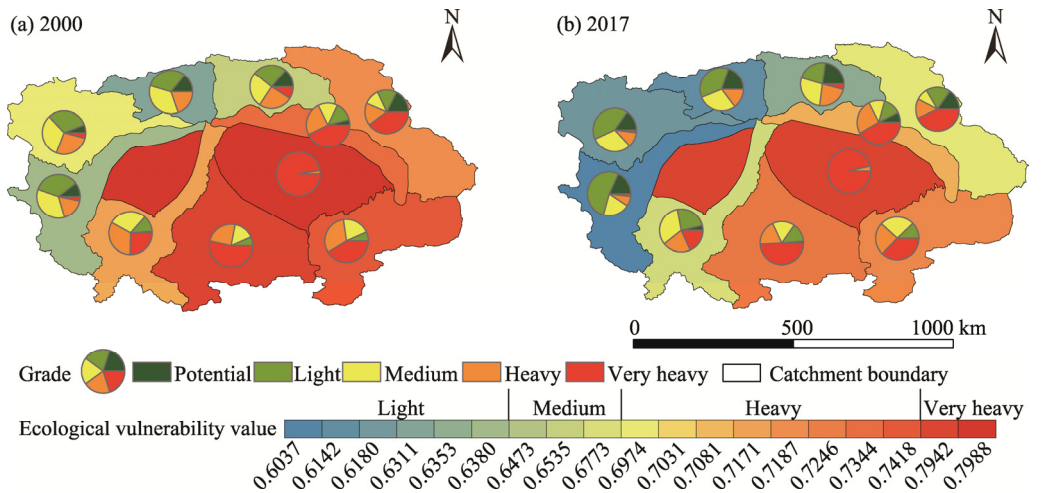

Fig. 3 Statistics of ecological vulnerability values at each catchment of the TRB in 2000 (a) and 2017 (b). Note that the pie charts show the proportion of different ecological vulnerability grades, and the ecological vulnerability values at each catchment represent the mean ecological vulnerability value of that catchment.

The statistics of ecological vulnerability based on LULC and geomorphic parameters (altitude and slope) are shown in Figure 4. In terms of land cover types, the cropland had lower value of ecological vulnerability than grassland and forestland did (Fig. 4a). The crops in the agricultural oases usually had abundant irrigation water, thus the vegetation cover of the crops exhibited weaker relationships with decreasing precipitation or severe drought. From the perspective of terrain parameters, the ecological vulnerability values had negative relations with altitude (Fig. 4b) and slope (Fig. 4c). The ecological environment of mid-mountain regions with an elevation of 2500–3500 m and a slope of 25°–35° was classified as being in good condition based on the lowest values of ecological vulnerability (0.645 (±0.048)–0.620 (±0.053)). However, the lowland regions with an elevation below 1500 m and a slope less than 5° had the most fragile ecological environments based on the highest ecological vulnerability values (0.724 (±0.097)–0.747 (±0.088)).

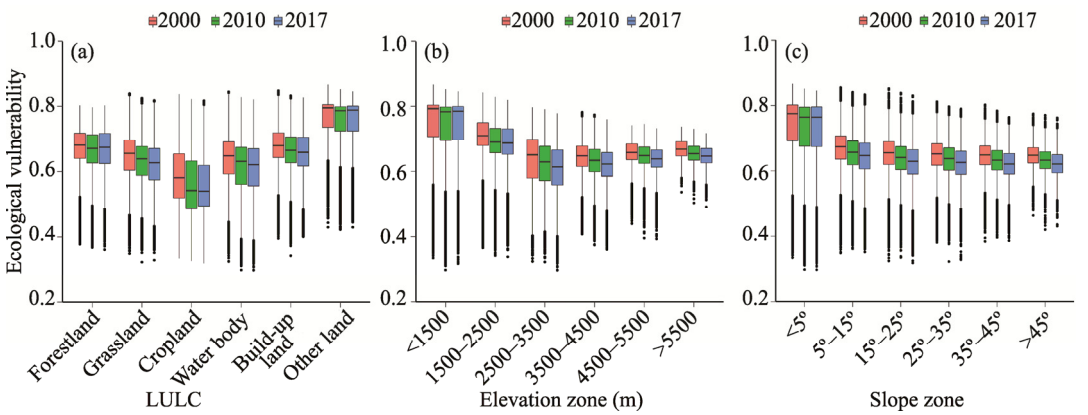

Fig. 4 Statistics of ecological vulnerability values in 2000, 2010, and 2017 based on LULC (a), elevation (b), and slope (c). Note that the black circles are outliers on each box; the central black line is the median; and the edges of the box are the upper and lower quartiles.

3.2 Spatial-temporal variations of ecological vulnerability

The distribution maps of ecological vulnerability during the periods of 2000–2010, 2010–2017, and 2000–2017 were used to analyze the spatial-temporal variations of ecological vulnerability in the TRB (Fig. 5). The negative ecological vulnerability values represent ecological improvement,

and the positive values indicate ecological degradation. From 2000 to 2010, approximately 36.06% of the total TRB area greatly improved (changes of ecological vulnerability in the range from –0.06 to –0.02), and 57.18% of the area was slightly improved (changes of ecological vulnerability in the range from –0.02 to 0.00) (Fig. 5d). The LULC types of these improved regions are alpine grassland and cropland (Fig. 5a). The regions of ecological degradation that accounted for 6.76% of the total area were mainly distributed in mountain regions of the Kaidu River catchment, the middle reaches of the Tarim River (Luntai County), and the cropland of the Qarqan River catchment (Qiemo County).

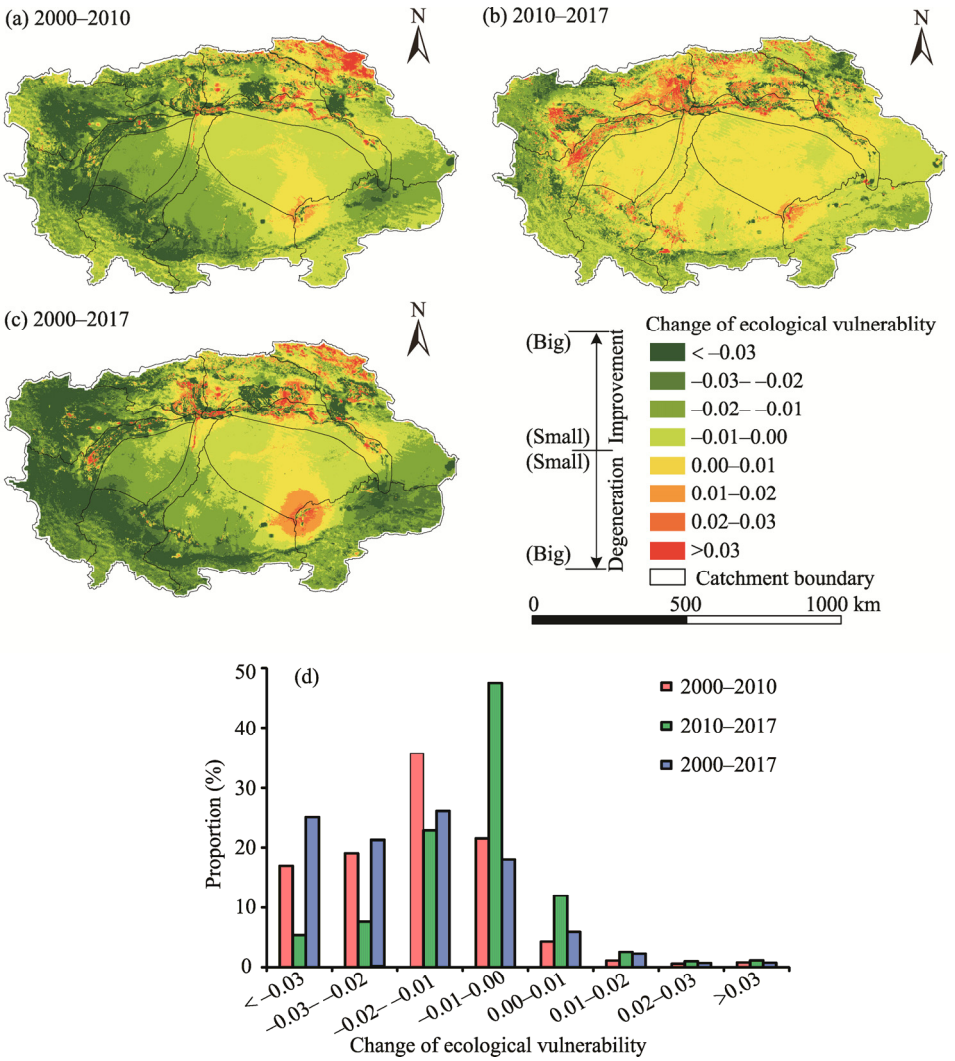

Fig. 5 Spatial-temporal distributions in the changes of ecological vulnerability in the TRB during 2000–2010 (a), 2010–2017 (b), and 2000–2017 (c), as well as the proportion of changed values for ecological vulnerability during 2000–2010, 2010–2017, and 2000–2017 (d).

From 2010 to 2017, the improvement degree of the ecological environment slowed down, with 12.97% of the total area greatly improving (Fig. 5d). The ecological environment of grassland in mountain ranges exhibited slight improvement, including the Kaidu River catchment, but that of cropland along the upstream river reaches was generally degraded (Fig. 5b). During the long period of 2000–2017, the greatly ecological improvement occurred in about 46.11% of the catchment area, but approximately 9.64% of the area showed ecological degradation (Fig. 5d). Significant ecological improvement mostly occurred in alpine grassland surrounding the

catchments, and the ecological environment of cropland along the river was also improved (Fig. 5c). The spatial distributions of ecological degeneration from 2000 to 2017 were similar to those from 2000 to 2010. In addition, the transition zone between cropland and forestland showed discontinuous degeneration in the Aksu River and Yarkant River catchments, and the desert riparian forest in the middle reaches of the Tarim River also showed significant degradation.

The spatial-temporal variations of ecological vulnerability grades in the TRB during 2000–2010, 2010–2017, and 2000–2017 are displayed in Figure 6a–c. Overall, approximately 80.00% of the total area maintained their grades without changes. Most of the ecological improvement regions were upgraded by one level.

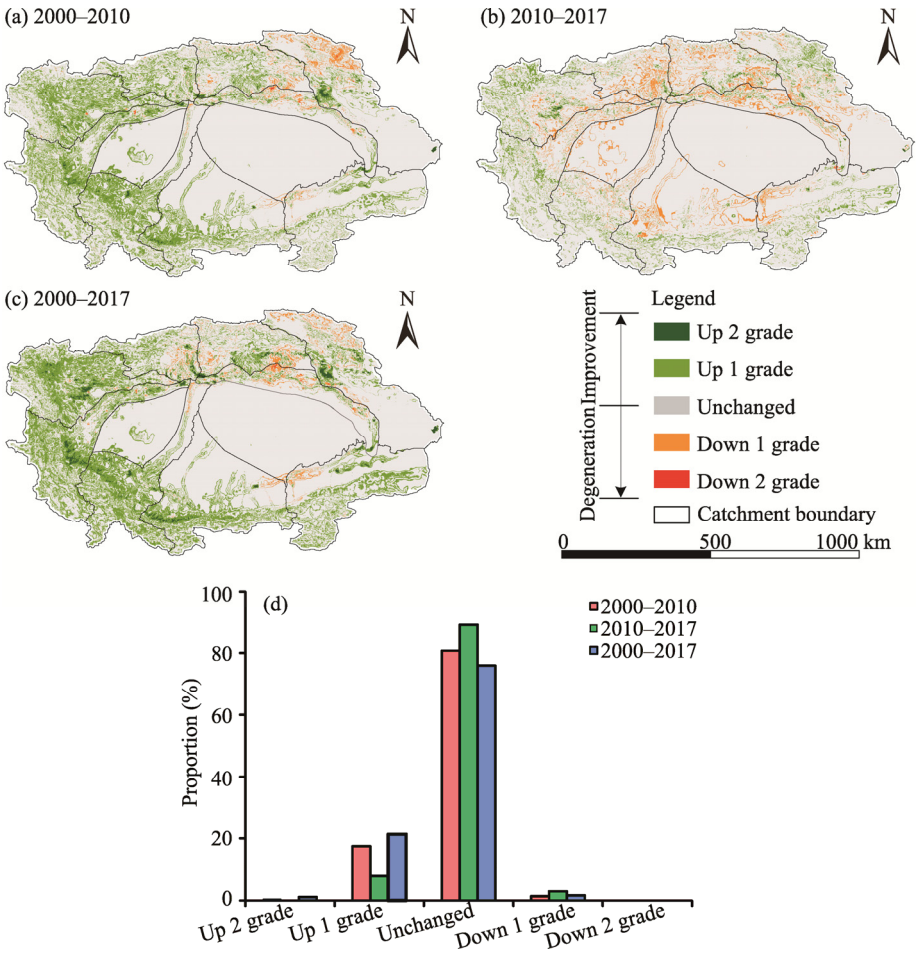

Fig. 6 Spatial-temporal distributions in the changes of ecological vulnerability grade in the TRB during 2000–2010 (a), 2010–2017 (b), and 2000–2017 (c), as well as the proportion of changed grades for ecological vulnerability during 2000–2010, 2010–2017, and 2000–2017 (d)

During 2000–2017, about 21.33% of the total area increased by one grade, while only 1.65% of the area decreased by one grade (Fig. 6d). The most significant improvement in the ecological environment was in the Kashgar River, Yarkant River, and Hotan River catchments. The regions where environmental improvements were increased by one level were mainly distributed in grassland of the West Tianshan Mountains, Karakoram Mountains, Kunlun Mountains, and Altun Mountains, as well as in alluvial plains in the Kaidu River, Weigan River, Kashgar River, Yarkant River, and Hotan River catchments. However, results showed that ecological vulnerability downgraded by one grade in the Middle Tianshan Mountains, in the middle reaches of the Tarim River, and in the southeast margin of the Taklimakan Desert (Qiemo County).

3.3 Impacts of driving factors on ecological vulnerability in the TRB

The influences of climatic, ecological, and socioeconomic factors on ecological vulnerability in the TRB were analyzed by *q*-values shown in Table 3. In the whole TRB, the impacts of ecological factors on ecological vulnerability were the greatest, while those of socioeconomic factors were the lowest (Table 3). The influences of each driving factor from high to low were: vegetation cover>PET>water density>precipitation>landscape diversity>AFT>population density>food production>soil erosion>livestock density. The vegetation cover had the greatest *q*-value of 0.5756, which could mainly explain the spatial heterogeneity of ecological vulnerability. PET, with a *q*-value of 0.2155, was the second most important driving factor. The *q*-values of water density and precipitation were all higher than 0.1000, showing that these two factors were relatively important driving factors. The *q*-values of population density, food production, and livestock density were all lower than 0.0100, indicating that these socioeconomic factors had the smaller impacts on ecological vulnerability.

Table 3 Contribution (*q*-values) of ten driving factors influencing ecological vulnerability in the TRB

Catchment	Contribution (*q*-value)									
	Climate indicator			Ecological indicator				Socioeconomic indicator		
	PRE	AFT	PET	LD	SE	VC	WD	FOOD	POP	LS
Total basin	0.1144	0.0505	0.2155	0.0950	0.0170	0.5756	0.1816	0.0235	0.0414	0.0095
Kaidu River	0.0003	0.0013	0.0098	0.2096	0.0511	0.5706	0.2217	0.1021	0.0562	0.1117
Weigan River	0.0399	0.0167	0.0615	0.1249	0.0086	0.7859	0.0370	0.0006	0.0326	0.0732
Aksu River	0.0395	0.0395	0.0409	0.1277	0.0178	0.6075	0.0465	0.0227	0.0380	0.0440
Kashgar River	0.0083	0.0214	0.0668	0.1625	0.0100	0.7152	0.1022	0.0675	0.0506	0.0567
Yarkant River	0.0409	0.0370	0.0606	0.0271	0.0113	0.6218	0.0814	0.0281	0.0247	0.0339
Hotan River	0.0356	0.2401	0.3084	0.0758	0.0189	0.6560	0.1830	0.0520	0.0809	0.1028
Mainstream	0.0229	0.0277	0.1020	0.1427	0.0025	0.6026	0.1103	0.0111	0.0079	0.0018
Kunlun Mountains	0.1546	0.1354	0.3304	0.0397	0.0101	0.6975	0.2687	0.0002	0.0084	0.0087
Qarqan River	0.0004	0.0360	0.5191	0.1587	0.0020	0.2598	0.0892	-	-	-

Note: -, no data.

In the catchments with better ecological environments (Weigan River, Aksu River, Kashgar River, and Yarkant River catchments), vegetation cover was the most important factor impacting the spatial-temporal variations in ecological vulnerability. It shows that better vegetation growth in mountainous regions of these catchments would improve the ecological environment. However, the PET had the highest influence on the spatial-temporal variations of ecological vulnerability in the Qarqan River catchment (*q*-value of 0.5191), followed by that in the Kunlun Mountains catchment (*q*-value of 0.3304) and Hotan River catchment (*q*-value of 0.3084), which implies that increased drought is one of the most important limitations of the ecological environment in these regions. In the Kaidu River and Hotan River catchments, livestock density played a more important role in the ecological environment, explaining 11.17% and 10.28% of the changes in ecological vulnerability, respectively, which indicates that overgrazing is the most important factor affecting ecological balance in mountain regions.

4 Discussion

4.1 Comparison of spatial-temporal variations in ecological vulnerability between the AHP-entropy method and vegetation index of the remote sensing dataset

A number of studies have found increasing trends in vegetation greenness for both grassland and cropland across most regions of Xinjiang based on the Moderate Resolution Imaging Spectroradiometer (MODIS) or the Global Inventory Monitoring and Modelling Studies (GIMMS) dataset over the past decades (Rong et al., 2016; Liu et al., 2018; Yao et al., 2019; He et al., 2021), and these results were consistent with our findings. The annual maximum value of the

MODIS EVI was taken as representative of vegetation greenness from 2000 to 2017 in the TRB (Fig. 7a). The result indicated that the regions distributed along the upstream rivers and cropland had more significantly increasing trends than those distributed in mountain ranges. The decreasing trends of the EVI were mainly located in grasslands of the Middle Tianshan Mountains, as well as in the middle reaches of the Tarim River. Overall, the spatial-temporal patterns of vegetation greenness represented by the MODIS EVI were similar to the ecological vulnerability results estimated by the AHP-entropy method in this study.

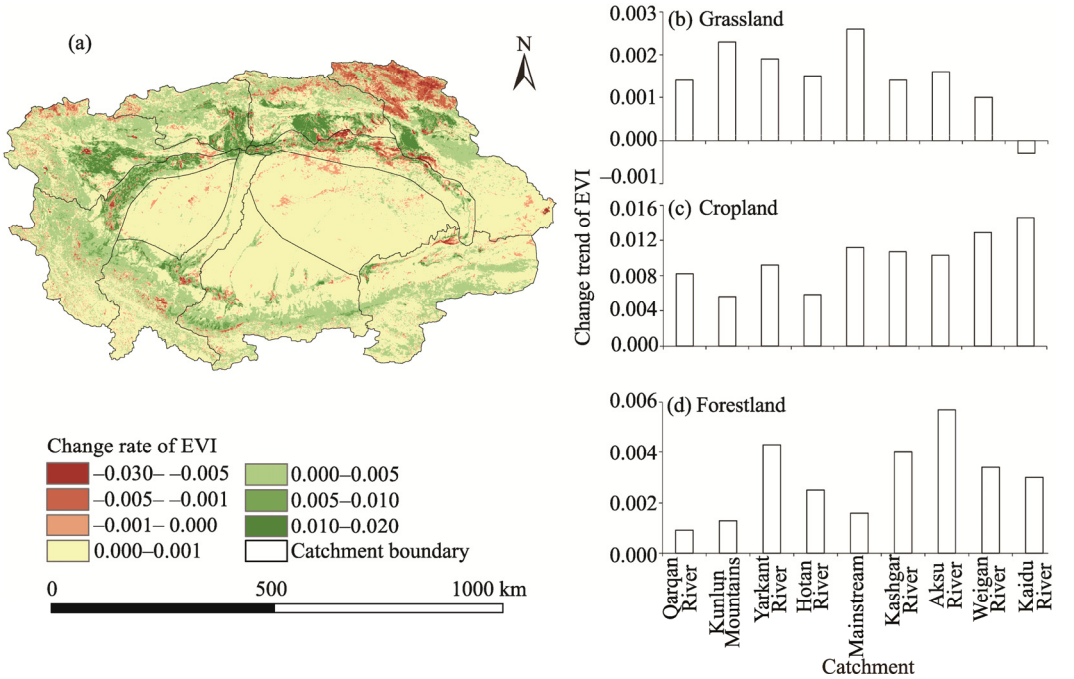

Fig. 7 Spatial distribution of the annual maximum MODIS enhanced vegetation index (EVI) trend from 2000 to 2017. (a), spatial distribution of the changed rates of EVI in the whole TRB; (b)–(d), statistical results for the change trends of EVI in grassland, cropland, and forestland in different catchments, respectively. Note that the positive value indicates increasing trend of vegetation growth, and negative value means decreasing trend of vegetation growth.

4.2 Spatial-temporal changes in ecological vulnerability of different LULC types

4.2.1 Spatial-temporal changes in ecological vulnerability of grassland

Except for the Kaidu River catchment, the other eight catchments experienced positive change trends of vegetation growth in grassland based on the MODIS EVI (Fig. 7b). The greening of alpine grasslands had positive effects on the ecological environment, especially in the upstream regions of the Kashgar River and Yarkant River catchments (Fig. 5c). The grassland in highlands or lowlands of arid regions was the most sensitive vegetation type to short-term climatic fluctuations and was most severely degraded by human activities (such as overgrazing or clearing) (Jiapaer et al., 2015). Many studies have indicated that the increased vegetation index of grassland is mainly due to increased precipitation instead of rising temperature in the arid regions of Northwest China (Yuan et al., 2015; Zhang et al., 2020). With the climate changing from warm-dry to warm-wet since the 1980s in Xinjiang (Shi et al., 2007), the increasing trends of vegetation growth in grassland have played a positive effect on the improvement of the ecological environment around the TRB, especially in the Karakoram Mountains, Kunlun Mountains, and Altun Mountains. In arid regions, grassland recovers from drought more easily when it receives supplemental water compared to shrubland (Bai et al., 2019); therefore, ecological water transport has positively promoted grassland regeneration in the middle and lower reaches of the Tarim River.

4.2.2 Spatial-temporal changes in ecological vulnerability of cropland

The MODIS EVI of cropland in the TRB rapidly increased from 0.16 (±0.03) to 0.31 (±0.12), especially in the Kaidu River and Weigan River catchments (Fig. 7b). This result is consistent with the results of ecological vulnerability assessments, which suggested that the ecological environment of cropland showed obvious improvement from 2000 to 2017 (Fig. 5c). Aggregated total area of grassland, cropland, and forestland in different catchments in 2000, 2010, and 2017, as well as aggregated total area of land transformation in different catchments are shown in Figure 8. The cropland was mainly distributed in the upstream of Kashgar River, Yarkant River, Weigan River, and Aksu River catchments, which accounted for 19.47%, 16.47%, 16.15%, and 15.91% of the total cropland area in the TRB, respectively (Fig. 8b). Recently, abundant fertilizer application, water-saving irrigation, and the construction of water conservancy facilities have promoted crop productivity and water use efficiency (Attia et al., 2021). From 2000 to 2017, nitrogenous fertilizer was increased by 30.00%, while the yields of grain crops (both wheat and maize) and cotton continuously increased at the rates of 0.103 and 0.077 t/(hm^2·a), respectively (Fig. 9a). The cropland here was deeply dependent on human management; thus, the ecological vulnerability of cropland continuously decreased, which might be related to the progress of agricultural management.

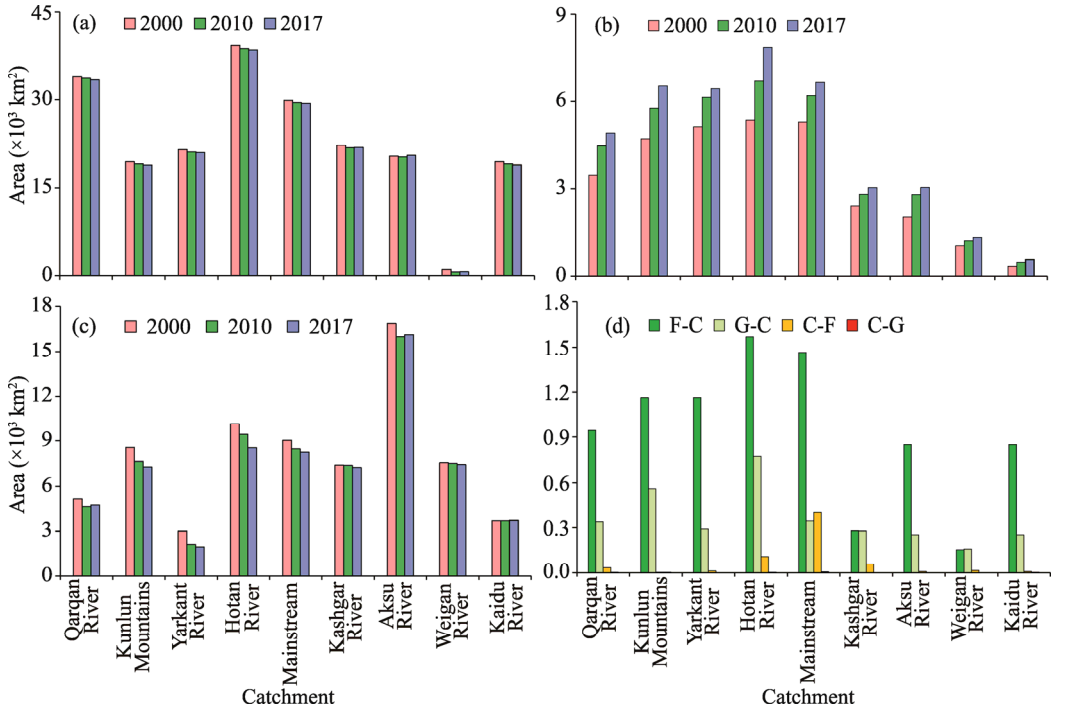

Fig. 8 Aggregated total area of grassland (a), cropland (b), and forestland (c) in different catchments in 2000, 2010, and 2017, as well as aggregated total area of land transformation in different catchments (d). F-C, transformation of forestland to cropland; G-C, transformation of grassland to cropland; C-F, transformation of cropland to forestland; C-G, transformation of cropland to grassland.

During the period of 2000–2017, the cropland area continuously increased from 2.98×10^3 to 4.04×10^3 km^2, and it was mainly converted from forestland and grassland. Agricultural reclamation was mainly concentrated in the upstream catchments (Kashgar River, Yarkant River, Aksu River, Weigan River, and Kaidu River catchments) and the upper and middle reaches of the Tarim River. The greatest agricultural reclamation occurred in the oases of Kashgar River and Yarkant River catchments, accounting for 40.00% of the total cropland area which converted from forestland (Fig. 8d). The significant increase in cropland converted from forestland implied that

more water resources would be consumed as agricultural irrigation, and less would be used by natural vegetation (Fig. 9b).

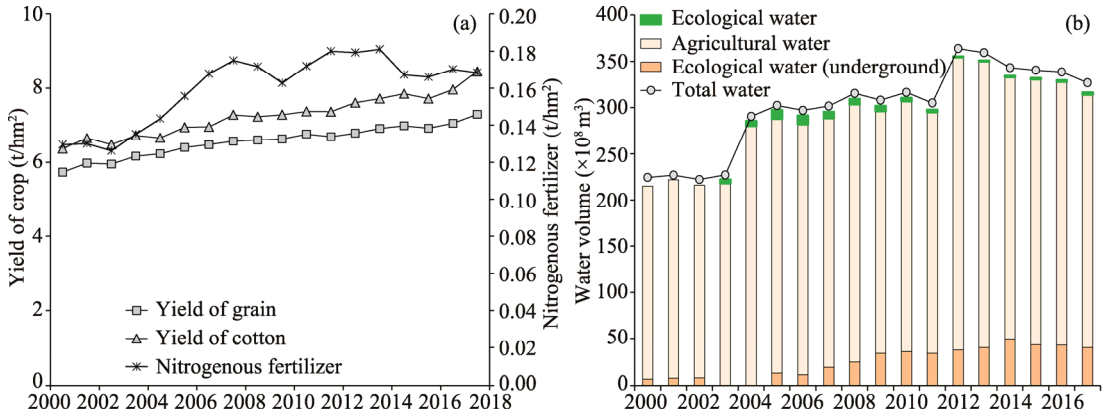

Fig. 9 Crop yield and nitrogenous fertilizer utilization (a) as well as water consumption for different uses (b) in the TRB from 2000 to 2017

4.2.3 Spatial-temporal changes in ecological vulnerability of forestland

The increased rate of MODIS EVI for forestland in the upstream catchments (Yarkant River, Kashgar River, and Aksu River catchments) was much higher than that in the Mainstream catchment (Fig. 7d). This result suggested that the ecological environment of forestland in the upstream catchments was higher than that in the desert riparian forest in the Mainstream catchment. Although the MODIS EVI of forestland in the Mainstream catchment showed obvious growth trends (Fig. 7d), we found sporadic degeneration of vegetation in the middle reaches of the Tarim River (Fig. 5a–c). The water transport dike in the middle stream of the Tarim River cut off the river overflow mechanism, which impacted the self-renewal of the desert riparian community and degraded the ecological environment. Guo et al. (2017) also noted the decreasing trends in the fractional vegetation along the middle stream of the Tarim River in 2000 and 2013, which was consistent with our study.

In the lower reaches of the Tarim River, the river runoff from the main branch and the Konqi River have generally raised the groundwater table and promoted the rapid regeneration of desert riparian forest within 300 m from the riverbank (Chen et al., 2010; Bao et al., 2017; Ling et al., 2019). However, the scope of restored riparian vegetation was closely related to that of the surface water receiving area. With the effect of the EWDP, which was conducted in a 'line style' pattern from 2000 to 2017, riparian vegetation was restored along the river channel and the ecological environment was improved (Fig. 5).

4.3 Impacts of climate change on ecological vulnerability

In the past half-century, both the annual mean temperature and annual precipitation in Xinjiang showed obvious growth trends based on data from local meteorological stations and reanalyzed datasets (Fang et al., 2013; He et al., 2020). Although the warming trend remained stable and precipitation slightly decreased in 1997–2015, the severity of drought increased, especially in South Xinjiang (Yao et al., 2018). In this study, AFT exhibited a significant increasing trend (0.008°C/a, $P<0.05$; Fig. 10a), but precipitation showed no significant increasing trend (1.6 mm/a, $P>0.05$; Fig. 10b) in the TRB during 2000–2017. The warming trend and no significant increased precipitation intensified the water resource stress in the TRB. Spatially, AFT and PET exhibited decreasing trends in the mountains around the TRB, but significant increasing trends were found in the middle reaches of the Tarim River (Fig. 10a and b). Precipitation showed increasing trends in the western regions but decreasing trends in the eastern regions during this period (Fig. 10b). There were also cooling and wetting trends in the high mountains and warming and drying trends in the low basins.

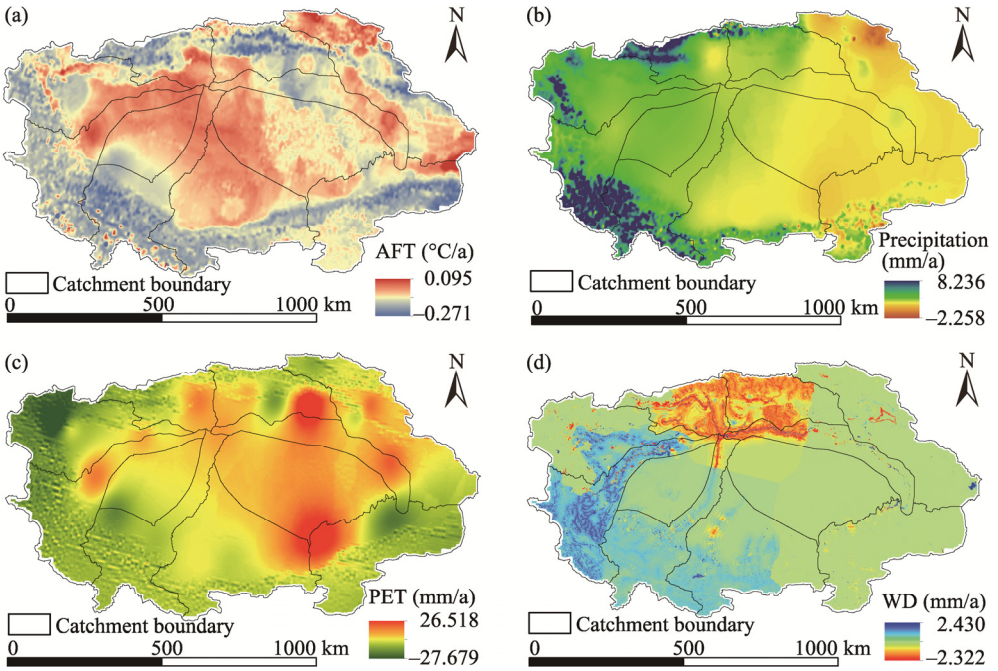

Fig. 10 Spatial changes in above-freezing temperature (AFT; a), precipitation (b), potential evapotranspiration (PET; c) and water density (WD; d) in the TRB from 2000 to 2017

Climate conditions would have beneficial effects on the ecological environment in the mountain grassland of upstream regions (e.g., Kashgar River, Yarkant River, Hotan River, and Kunlun Mountains catchments) with less human activities (Fig. 5c). However, the increased AFT and decreased precipitation in the Middle Tianshan Mountains would aggravate the degeneration of overgrazing grassland and have a negative effect on the ecological environment. We also found that significantly increasing PET occurred in the middle and lower reaches of the Tarim River (Luntai and Yuli counties), as well as around the southern edge of the desert (Qiemo County) (Fig. 10c). According to previous studies, the PET based on ground-based meteorological stations around the TRB also exhibited an increasing trend from 1994 to 2010 due to the increasing wind speed and vapor pressure deficit (Li et al., 2013; Dong et al., 2020), which was consistent with our results. Moreover, the increased irrigation water withdrawal in the agricultural oases may have a positive effect on PET (Han et al., 2011).

4.4 Impacts of changes in water resources on ecological vulnerability

Climate warming has resulted in significant growth trends of river runoff since 1960 in the headwaters of the Tarim River (Xu et al., 2010; Li et al., 2020; Wang et al., 2021). Snow and glacier meltwater are the primary sources of runoff in the Tarim River, accounting for 48.20% of the total water volume (Chen, 2007). Recently, the runoff of the Kaidu River and Aksu River supplied by rainfall and seasonal snowmelt water in the Middle Tianshan Mountains showed decreasing trends, which might be related to the decreases in precipitation (Deng et al., 2019). In contrast, the effect of glacier meltwater resulting from air temperature on runoff would be more remarkable in the Karakoram Mountains and Kunlun Mountains. Especially in the Yarkant River, where the contribution of glacier meltwater to runoff was about 50.00%, the significantly rising summer temperature has accelerated glacial shrinkage and increased runoff from 1996 to 2006 (Yao et al., 2018).

In this study, the water density indicator variations showed that the water resource in the western regions of the TRB was the most abundant (Yarkant River and Kashgar River catchments). We also found that the values of the water density indicator significantly increased in the Yarkant River, Kashgar River, Hotan River, and Kunlun Mountains catchments, but

decreased in the Weigan River and Aksu River catchments (Fig. 10d). This result was consistent with the variations in runoff in the Aksu River, Yarkant River, and Hotan River, which are the major source rivers in the TRB. The decreased runoff and increased cropland area as well as agricultural water might increase the water stress in the northern catchments of the TRB. However, the increased runoff would provide more water resources for natural vegetation and agricultural irrigation in the western and southwestern regions.

The agricultural water in the TRB, accounting for 96.50% of the total water consumption, increased from 215.00×10^8 m^3 in 2000 to 313.56×10^8 m^3 in 2017 (Fig. 9b). More groundwater was used as agricultural water, which increased from 13.13×10^8 m^3 in 2005 to 40.49×10^8 m^3 in 2017 (Fig. 9b). The increased exchange groundwater dynamic was significantly altered by the application of water-saving irrigation (Zhang et al., 2014). However, the water saved by drip irrigation was used to expand the cropland area, and it stressed the ecological water use in the lower reaches of the Tarim River. The ecological water remained at a higher level above the mean value (3.65×10^8 m^3) during 2003–2010, and then decreased to the lowest value of 1.20×10^8 m^3 in 2012 with progressive agricultural water consumption (Fig. 9b). The area of desert riparian forest in the Mainstream catchment was the greatest, accounting for 23.34% of the total forestland area (Fig. 8c), and these forestlands were more reliant on ecological water transport. As it requires a wet environment for germination and seedling growth, river overflow could activate crown seeds of plants and soil seeds in the soil seed bank (Xu et al., 2009; Zhou et al., 2020).

4.5 Impacts of socioeconomic changes on ecological vulnerability

As shown in Table 3, livestock played the most significant role in ecological vulnerability in the Kaidu River catchment among the TRB. The grassland area in the Kaidu River catchment ranked the second largest in the TRB (Fig. 8a), and it is also one of the important animal husbandry bases in Xinjiang. The overgrazing capacity in spring-autumn pastures increased from 30.10% to 50.00% during 1985–2007, with most meadow overloads even exceeding 100.00% in the Bayanbulak grassland of the Kaidu River catchment (Jiapaer et al., 2015). Overgrazing decreased grassland quality and retarded grassland restoration, causing the ecological environment in the Middle Tianshan Mountains to degrade continually.

5 Conclusions and suggestions

In this study, ten climatic, ecological, and socioeconomic indicators were selected to estimate ecological vulnerability in the TRB using the AHP-entropy method in 2000, 2010, and 2017. The results showed that the ecological environment was improved in most regions of the TRB, and the degree of ecological improvement was decreased from the northwestern regions to the southeastern regions. Vegetation cover and PET were the obvious driving factors, explaining 57.56% and 21.55% of the changes in ecological vulnerability across the TRB, respectively. Climate change is beneficial to the improvement of the ecological environment in most mountainous regions, but overgrazing aggravates grassland degradation in the Kaidu River catchment. The ecological environment of agricultural oases showed obvious improvement with more appropriate agricultural management technologies. However, the oasis-desert ecotones displayed sporadic degradation as cropland was reclaimed and under intensive drought. Therefore, it is urgent to make rational use of water and land resources in agricultural oases, and moderate land reclamation should be executed in the western and southwestern regions with abundant water resources. This study provides a comprehensive framework for a better understanding of ecological vulnerability at the basin scale and directly supports ecological managers and governments with decision-making in similar arid and semi-arid areas with limited water resources and fragile ecological environments.

We suggested the different measures of ecological protection and restoration in the TRB based on the different characteristics of ecological vulnerability, as follows. Agricultural development should be strictly controlled and water use efficiency should be enhanced in the agricultural oases of the Aksu River and Weigan River catchments to weaken the decreased water resources and

intensified drought. In the mountain grassland of the Kaidu River catchment, measures should be actively taken to restore the grassland and rebuild the forage-livestock balance, such as grazing blocked by fencing, rotational grazing, and compensatory seed planting. In the western regions (Yarkant River and Kashgar River catchments) and southwestern regions (Hotan River catchment) with abundant water resources, the reclamation of cropland converted from grassland and forestland should be moderate so that the ecological water flow into the main branch of Tarim River is not disrupted. In the Mainstream catchment, more attention should be given to the intensive implementation of forest rehabilitation from agriculture and the protection of seedlings of *Populus euphratica* forest to recover more natural vegetation cover and water body area.

Acknowledgements

This research was supported by the National Key Research and Development Plan of China (2017YFB0504204), the CAS Interdisciplinary Innovation Team (JCTD-2019–20), the Tianshan Innovation Team (2020D14016), and the National Natural Science Foundation of China (U2003201).

References

Amiri V, Rezaei M, Sohrabi N. 2014. Groundwater quality assessment using entropy weighted water quality index (EWQI) in Lenjanat, Iran. Environmental Earth Sciences, 72: 3479–3490.

Attia A, El-Hendawy S, Al-Suhaibani N, et al. 2021. Evaluating deficit irrigation scheduling strategies to improve yield and water productivity of maize in arid environment using simulation. Agricultural Water Management, 249: 106812, doi: 10.1016/j.agwat.2021.106812.

Bai J, Shi H, Yu Q, et al. 2019. Satellite-observed vegetation stability in response to changes in climate and total water storage in Central Asia. Science of the Total Environment, 659: 862–871.

Bao A M, Huang Y, Ma Y G, et al. 2017. Assessing the effect of EWDP on vegetation restoration by remote sensing in the lower reaches of Tarim River. Ecological Indicators, 74: 261–275.

Beroya-Eitner, M A, 2016. Ecological vulnerability indicators. Ecological Indicators, 60: 329–334.

Bestelmeyer B T, Okin G S, Duniway M C, et al. 2015. Desertification, land use, and the transformation of global drylands. Frontiers in Ecology and the Environment, 13: 28–36.

Chen Y N, Li W H, Xu C C, et al. 2007. Effects of climate change on water resources in Tarim River Basin, Northwest China. Journal of Environmental Sciences, 19(4): 488–493.

Chen Y N, Chen Y P, Xu C C, et al. 2010. Effects of ecological water conveyance on groundwater dynamics and riparian vegetation in the lower reaches of Tarim River, China. Hydrological Processes, 24: 170–177.

Department of Water Resources of Xinjiang Uygur Autonomous Region. 2000. Xinjiang Water Resources Bulletin. [2020-09-01]. http://slt.xinjiang.gov.cn/. (in Chinese)

Department of Water Resources of Xinjiang Uygur Autonomous Region. 2010. Xinjiang Water Resources Bulletin. [2020-09-01]. http://slt.xinjiang.gov.cn/. (in Chinese)

Department of Water Resources of Xinjiang Uygur Autonomous Region. 2017. Xinjiang Water Resources Bulletin. [2020-09-01]. http://slt.xinjiang.gov.cn/. (in Chinese)

Deng H, Chen Y, Li Q, et al. 2019. Loss of terrestrial water storage in the Tianshan mountains from 2003 to 2015. International Journal of Remote Sensing, 1608392, doi: 10.1080/01431161.2019.1608392.

Deng M J, Zhou H Y, Xu H L, et al. 2016, Research on the ecological operation in the lower reaches of Tarim River based on water conveyance. Scientia Sinica Technologica, 46: 864–876. (in Chinese)

Dong Q, Wang W, Shao Q, et al. 2020. The response of reference evapotranspiration to climate change in Xinjiang, China: Historical changes, driving forces, and future projections. International Journal of Climatology, 40: 235–254.

Du Y W, Gao K. 2020. Ecological security evaluation of marine ranching with AHP-entropy-based TOPSIS: A case study of Yantai, China. Marine Policy, 122: 104223, doi: 10.1016/j.marpol.2020.104223.

Dzeroski S. 2001. Applications of symbolic machine learning to ecological modelling. Ecological Modelling, 146: 263–273.

Enea M, Salemi G. 2001. Fuzzy approach to the environmental impact evaluation. Ecological Modelling, 136: 131–147.

Fang S, Yan J, Che M, et al. 2013. Climate change and the ecological responses in Xinjiang, China: Model simulations and data analyses. Quaternary International, 311: 108–116.

Groisman P, Bulygina O, Henebry G, et al. 2018. Dryland belt of Northern Eurasia: contemporary environmental changes and

their consequences. Environmental Research Letters, 13: 115008, doi: 10.1088/1748–9326/aae43c.

Guo B, Zang W Q, Luo W. 2020. Spatial-temporal shifts of ecological vulnerability of Karst Mountain ecosystem-impacts of global change and anthropogenic interference. Science of the Total Environment, 741: 140256, doi: 10.1016/j.scitotenv.2020.140256.

Guo H, Jiapaer G, Bao A M, et al. 2017. Effects of the Tarim River's middle stream water transport dike on the fractional cover of desert riparian vegetation. Ecological Engineering, 99: 333–342.

Han J J, Wang J P, Liang C, et al. 2021. Driving factors of desertification in Qaidam Basin, China: An 18-year analysis using the geographic detector model. Ecological Indicators, 124: 107404, doi: 10.1016/j.ecolind.2021.107404.

Han S J, Hu H P, Yang D W, et al. 2011. Irrigation impact on annual water balance of the oases in Tarim Basin, Northwest China. Hydrological Processes, 25: 167–174.

Hao X M, Li W H. 2014. Impacts of ecological water conveyance on groundwater dynamics and vegetation recovery in the lower reaches of the Tarim River in northwest China. Environmental Monitoring and Assessment, 186: 7605–7616.

He B B, Sheng Y, Cao W, et al. 2020. Characteristics of climate change in northern Xinjiang in 1961–2017, China. Chinese Geographical Science, 30(02): 249–265.

He P X, Sun Z J, Han Z M, et al. 2021. Dynamic characteristics and driving factors of vegetation greenness under changing environments in Xinjiang, China. Environmental Science and Pollution Research, doi: 10.1007/s11356-021-13721-z.

Hinkel J, 2011. "Indicators of vulnerability and adaptive capacity": Towards a clarification of the science-policy interface. Global Environmental Change, 21(1): 198–208.

Huang J P, Yu H P, Guan X D, et al. 2016. Accelerated dryland expansion under climate change. Nature Climate Change, 6: 166–171.

Jiapaer G, Liang S L, Yi Q X, et al. 2015. Vegetation dynamics and responses to recent climate change in Xinjiang using leaf area index as an indicator. Ecological Indicators, 58: 64–76.

Lei Y, Jiang D, Yang X H, et al. 2007. The water distribution model application based on spatial information technology. Geo-Information Science, 9: 64–69. (in Chinese)

Li Z, Chen Y N, Shen Y J, et al. 2013. Analysis of changing pan evaporation in the arid region of Northwest China. Water Resources Research, 49: 2205–2212.

Li Z H, Shi X G, Tang Q H, et al. 2020. Partitioning the contributions of glacier melt and precipitation to the 1971–2010 runoff increases in a headwater basin of the Tarim River. Journal of Hydrology, 583: 124579, doi: 10.1016/j.jhydrol.2020.124579.

Ling H B, Guo B, Zhang G P, et al. 2019. Evaluation of the ecological protective effect of the "large basin" comprehensive management system in the Tarim River basin, China. The Science of the total environment, 650: 1696–1706.

Liston G E, Elder K. 2006. A meteorological distribution system for high-resolution terrestrial modeling (MicroMet). Journal of Hydrometeorology, 7: 217–234.

Liu Y, Li L H, Chen X, et al. 2018. Temporal-spatial variations and influencing factors of vegetation cover in Xinjiang from 1982 to 2013 based on GIMMS-NDVI3g. Global and Planetary Change, 169: 145–155.

Ludovisi A. 2014. Effectiveness of entropy-based functions in the analysis of ecosystem state and development. Ecological Indicators, 36: 617–623.

Nachtergaele F, Velthuizen H V, Verelst L, et al. 2009. Harmonized World Soil Database (version 1.1). FAO, Rome, Italy and IIASA, Laxenburg, Austria.

Nandy S, Singh C, Das K K, et al. 2015. Environmental vulnerability assessment of eco-development zone of Great Himalayan National Park, Himachal Pradesh. Ecological Indicators, 57: 182–195.

Nguyen A K, Liou Y A, Li M H, et al. 2016. Zoning eco-environmental vulnerability for environmental management and protection. Ecological Indicators, 69: 100–117.

Nyimbili P H, Erden T. 2020. A hybrid approach integrating Entropy-AHP and GIS for suitability assessment of urban emergency facilities. International Journal of Geo-Information, 9: 419, doi: 10.3390/ijgi9070419.

Pan G B, Xu Y P, Yu Z H, et al. 2015. Analysis of river health variation under the background of urbanization based on entropy weight and matter-element model: A case study in Huzhou City in the Yangtze River Delta, China. Environmental Research, 139: 31–35.

Renard K G, Foster G R, Weesies G A. et al. 1991. RUSLE: Revised universal soil loss equation. Journal of Soil and Water Conservation, 46(1): 30–33.

Saaty T L, 2001. The analytic hierarchy process. In: Gass S I, Harris C M. Encyclopedia of Operations Research and Management Science. New York: Springer, 287.

Silva M M, Poleto T, Lucio C E S, et al. 2016. A grey theory based approach to big data risk management using FMEA. Mathematical Problems in Engineering, 9175418, doi: 10.1155/2016/9175418.

Shi Y F, Shen Y P, Kang E, et al. 2007. Recent and future climate change in northwest China. Climatic Change, 80: 379–393.

Shi Y S, Li J Q, Xie M Q, 2018. Evaluation of the ecological sensitivity and security of tidal flats in Shanghai. Ecological Indicators, 85: 729–741.

Wang J F, Zhang T L, Fu B J, 2016. A measure of spatial stratified heterogeneity. Ecological indicators, 67: 250–256.

Wang X L, Luo Y, Sun L, et al. 2021. Different climate factors contributing for runoff increases in the high glacierized tributaries of Tarim River Basin, China. Journal of Hydrology: Regional Studies, 36: 100845, doi: 10.1016/j.ejrh.2021.100845.

Wei S G, Dai Y J, Liu B Y, et al. 2012. A soil particle-size distribution dataset for regional land and climate modelling in China. Geoderma, 171: 85–91.

Williams L R R, Kaputska L A. 2000. Ecosystem vulnerability: a complex interface with technical components. Environmental Toxicology and Chemistry, 19: 1055–1058.

Wu B F, Zeng Y, Qian J K. 2017. Land Cover Atlas of the People's Republic of China (1:1000,000). Beijing: SinoMaps Press. (in Chinese)

Xinjiang Uygur Autonomous Region Bureau of Statistics. 2000–2017. Xinjiang Statistical Yearbook. Beijing: China Statistics Press. (in Chinese)

Xu H L, Ye M, Li J M. 2009. The ecological characteristics of the riparian vegetation affected by river overflowing disturbance in the lower Tarim River. Environmental Geology, 58: 1749–1755.

Xu Z, Liu Z, Fu G, et al. 2010. Trends of major hydroclimatic variables in the Tarim River basin during the past 50 years. Journal of Arid Environments, 74: 256–267.

Xue L Q, Jing W, Zhang L C, et al. 2018. Spatiotemporal analysis of ecological vulnerability and management in the Tarim River Basin, China. Science of the Total Environment, 649: 876–888.

Yao J Q, Zhao Y, Chen Y N, et al. 2018. Multi-scale assessments of droughts: A case study in Xinjiang, China. Science of the Total Environment, 630: 444–452.

Yao J Q, Hu W F, Chen Y N, et al. 2019. Hydro-climatic changes and their impacts on vegetation in Xinjiang, Central Asia, Science of the Total Environment, 660: 724–732.

Yu T, Bao A M, Xu W Q, et al. 2020. Exploring variability in landscape ecological risk and quantifying its driving factors in the Amu Darya Delta. International Journal of Environmental Research and Public Health, 17: 79, doi: 10.3390/ijerph17010079.

Yuan X L, Li L H, Chen X. 2015. Increased grass NDVI under contrasting trends of precipitation change over North China during 1982–2011. Remote Sensing Letters, 6: 69–77.

Zhang F, Wang C H, Wang Z H. 2020. Response of natural vegetation to climate in dryland ecosystems: a comparative study between Xinjiang and Arizona. Remote Sensing, 12: 3567, doi: 10.3390/rs1221356.

Zhang L, Li X S, Yuan Q Z, et al. 2014. Object-based approach to national land cover mapping using HJ satellite imagery, Journal of Applied Remote Sensing, 8: 083686, doi: 10.1117/1.JRS.8.083686.

Zhang Z, Hu H, Tian F, et al. 2014. Groundwater dynamics under water-saving irrigation and implications for sustainable water management in an oasis: Tarim River basin of western China. Hydrology and Earth System Sciences, 18: 3951–3967.

Zhao J C, Ji G X, Tian Y, et al. 2018. Environmental vulnerability assessment for mainland China based on entropy method. Ecological Indicators, 91: 410–422.

Zhou H H, Chen Y N, Zhu C G, et al. 2020. Climate change may accelerate the decline of desert riparian forest in the lower Tarim River, Northwestern China: Evidence from tree-rings of *Populus euphratica*. Ecological Indicators, 111: 105997, doi: 10.1016/j.ecolind.2019.105997.

Zhu Y X, Tian D Z, Yan F. 2020. Effectiveness of entropy weight method in decision-making. Mathematical Problems in Engineering, 2020, doi: 10.1155/2020/3564835.

Zou T H, Yoshino K. 2017. Environmental vulnerability evaluation using a spatial principal components approach in the Daxing'anling region, China. Ecological Indicators, 78: 405–415.

Appendix

Table S1 Indicator system of ecological vulnerability in Tarim River Basin

Vulnerability index	Indicator	Calculation formula	Formula description
Climate indicator	Above-freezing temperature (AFT) (unit: °C)	$AFT = \frac{\sum_{i=1}^{n} T_i}{n}$	T_i is the daily temperature above zero (°C); and n is the number of corresponding days.
	Precipitation (PRE; unit: mm)	$PRE = \sum_{i=1}^{n} PRE_i$	PRE_i is the daily precipitation on the i^{th} day (mm); and n is the day number (n=365).
	Potential evapotranspiration (PET; unit: mm)	$PET = \frac{0.408\Delta(R_n - G) + r\frac{900}{T+273}U_2(e_s - e_a)}{\Delta + r(1 + 0.34U_2)}$	R_n is the net radiation (MJ/(m^2•d)); G is the soil heat flux (MJ/(m^2•d)); r is the psychrometric constant (kPa/°C); T is the temperature (°C); U_2 is the wind speed (m/s); e_s is the saturation vapour pressure (kPa); e_a is the actual vapour pressure (kPa); and Δ is the slope of vapour pressure curve (kPa/°C).
Ecological indicator	Vegetation cover (VC)	$VC = \frac{EVI - EVI_0}{EVI_s - EVI_0}$	EVI_s is the value at highly dense vegetation fraction; and EVI_0 is that value for bare soil.
	Soil erosion (SE; unit: t/hm^2)	$SE = R \times K \times LS \times C \times P$	R is the rainfall erosivity factor (t/hm^2); K is the soil erodibility factor; LS is the topographic factor; C is the vegetation cover factor; and P is the erosion control practices factor.
	Landscape diversity (LD)	$LD = -\sum_{i=1}^{m}(P_i \times \ln P_i)$	P_i is the proportion of the area for the patch type i in the landscape (%); and m is the number of patch types in the landscape.
	Water density (WD; Unit: mm)	$WD = (L_r + S_l + Q_w \times W_Q)/3$	L_r is the length of river (m); S_l is the area of water body (m^2); Q_w is the available water resource (m^3); and W_Q is the weight of available water resource.
Socioeconomic indicator	Population density (POP; unit: person/hm^2)	$POP = \frac{POP_{total}}{A}$	POP_{total} is the urban and rural population (person); and A is the area of county (hm^2).
	Food production (FOOD; unit: calorie/hm^2)	$FOOD = \frac{\sum_{i=1}^{n}(100 \times M_i \times EP_i \times E_i)}{A}$	i is the production category numbered from 1 to n; M_i is the product yield per category i (t); EP_i is the edible percentage of the product by category (%); E_i is the calories per 100 g of the product (calorie/g); and A is the area of county (hm^2).
	Livestock density (LS; unit: head/hm^2)	$LS = \frac{\sum_{i=1}^{n}(LS_i \times L_i)}{A}$	i is the livestock type numbered from 1 to n; LS_i is the livestock of type i (head); L_i is the converted ratio of standard sheep; and A is the area of county (hm^2).